ChemPubSoc Europe

DOI: 10.1002/cphc.201900653

CHEMPHYSCHEM Articles

Special Issue

Effects of Capping Agents on the Oxygen Reduction Reaction Activity and Shape Stability of Pt Nanocubes

Isaac A. Safo,[a] Carsten Dosche,[a] and Mehtap Özaslan*[a, b]

We investigated the formation of Pt nanocubes (NCs) and their electrocatalytic oxygen reduction reaction (ORR) properties and structural stability using two different capping agents, namely, polyvinylpyrrolidone (PVP) and oleylamine (OAm). The mono-dispersity of the obtained Pt NCs and their interactions with PVP and OAm were analyzed by transmission electron microscopy (TEM), energy dispersive X-ray spectroscopy (EDX), X-ray photoelectron spectroscopy (XPS), Fourier-transformed infrared spectroscopy (FTIR) and thermogravimetric analysis (TGA). The TEM data show a high mono-dispersity (82%) and a large mean particle size (9-10 nm) for the Pt NCs obtained by the oleylamine-assisted method compared to those prepared via the PVP-assisted procedure (68%, 6–7 nm). FTIR, XPS, and TGA data show that PVP and OAm still remain at the Pt surface, despite washing. Interestingly, the OAm-capped Pt NCs show significantly higher electrochemically active surface area (ECSA) and ORR activity than the PVP-capped ones. An accelerated stress protocol, however, reveals that the OAm-capped NCs possess a poor structural stability during electrochemical cycling. The loss of a defined surface arrangement in the NCs is connected with a transformation into a near-spherical particle shape. In contrast, the PVP-capped NCs mainly retain their particle shape due to their strong capping behavior. In addition, we have developed a degradation model for NCs as a function of electrochemical parameters such as upper potential and cycle number. Altogether, we provide fundamental insights into the electronic interactions between capping agent and Pt NCs and the role of the adsorption strength of the capping agent in improving the electrochemical ORR performance as well as the structural stability of shape-controlled nanoparticles.

1. Introduction

Platinum-based nanoparticles are among the state-of-the-art electrocatalysts used as electrode materials for applications of polymer electrolyte fuel cells (PEFCs).[1–3] However, high loadings of very costly and scare Pt are still required to accelerate the sluggish kinetics of the oxygen reduction reaction (ORR) which hinders the broad commercialization of PEFCs.[4,5] In the last 25 years, many research groups have focussed on the design of highly efficient and robust Pt-based ORR electrocatalysts. Recently, shape-controlled Pt-based nanoparticles have emerged as one of the promising ORR electrocatalysts with improved performance.[6–9] The activity and selectivity of structure-sensitive reactions like ORR can be optimized by tailoring the surface arrangement and structure of shaped-controlled nanomaterials.[10–12] The very sensitive structure-activity relationship for ORR has extensively been investigated using well-defined Pt single crystal electrodes.[13,14] Shape-controlled Pt nanoparticles have a large potential to bridge the knowledge gap between model single crystal systems and carbon-supported Pt nanoparticles of 2–3 nm for ORR.[15] In addition, a shape-controlled nanoparticle presents well-defined facets which modify the adsorption of reactants to the surface, the bond cleavage to form intermediates and the desorption of products from the electrode surface.[16,17]

Generally, the preparation of shape-controlled nanoparticles requires the use of capping agents to stabilize and promote the evolution of specific surface arrangements and structures during nucleation and growth of Pt nanoparticles.[18,19] After synthesis, residuals of capping agents, yet, might block the utilization and accessibility to the available active sites on the surface of shape-controlled Pt nanoparticles and cause a catalyst deactivation/poisoning.[20,21] Recently, many research groups have applied solvent washing,[22] thermal annealing in air,[23,24] electrochemical cleaning,[25] UV-ozone cleaning,[26] plasma treatment,[27] and washing in acetic acid[28] media to remove capping agent like PVP from Pt surfaces. The critical challenge is to retain the specific surface structure and mono-dispersity of shape-controlled Pt nanoparticles. For example, UV-ozone and thermal annealing of PVP-capped Pt nanoparticles lead to carbonaceous residues which strongly affect the performance for methanol oxidation reaction.[29] Definitely, clean particle surfaces are an indispensable requirement for any structure-activity-selectivity correlation studies using shape-controlled nanoparticles. Thus, it is of fundamental and technological importance to develop efficient cleaning procedures for nanoparticles with well-defined surface orientation to remove capping agent residues prior to electrocatalytic applications. However, the removal of surfactants from nanoparticles without

[a] Dr. I. A. Safo, Dr. C. Dosche, Prof. Dr. M. Özaslan
Physical Chemistry, Carl von Ossietzky University of Oldenburg, 26129 Oldenburg, Germany
E-mail: mehtap.oezaslan@uol.de
m.oezaslan@tu-braunschweig.de
[b] Prof. Dr. M. Özaslan
Institute of Technical Chemistry, Technical University of Braunschweig, 38106 Braunschweig, Germany.

Supporting information for this article is available on the WWW under https://doi.org/10.1002/cphc.201900653

An invited contribution to a Special Issue on Electrocatalysis

© 2019 The Authors. Published by Wiley-VCH Verlag GmbH & Co. KGaA. This is an open access article under the terms of the Creative Commons Attribution Non-Commercial NoDerivs License, which permits use and distribution in any medium, provided the original work is properly cited, the use is non-commercial and no modifications or adaptations are made.

any modification of the specific surface orientation of nanoparticles is often not a trivial issue.

A critical description is the strength of adsorption behaviour of capping agent on the Pt surface. For example, polyvinylpyrrolidone (PVP)[30] is able to strongly adsorb on the metallic surface. Therefore, various cleaning procedures like UV/ozone radiation,[26] polar organic solvent washing,[22] acid washing[31] and oxidative thermal treatment[32] have been applied to remove PVP residues from the surface of Pt nanocubes (NCs). In contrast, oleylamine (OAm) which is well-known as moderate capping agent can be easily removed after synthesis by soft techniques like solvent washing using acetone, methanol/ethanol and hexane.[33,34] The complete removal of capping agents may expose "naked" Pt surface atoms to highly corrosive electrochemical fuel cell conditions, allowing the study of surface-sensitive reactions like ORR. Therefore, optimal strategies to fabricate shape-controlled nanoparticles with clean surface arrangement and structure for electrocatalytic applications are necessary. Another challenge associated with shape-controlled nanoparticles is their stability of particle shape and long-term catalytic performance under electrochemical fuel cell conditions. Indeed, the presence of capping agent from the synthesis strongly influences the electrochemical and structural aging processes of shape-controlled Pt nanoparticles. For example, Markovic et al.[21] have reported that cubic nanoparticles synthesized by oleylamine loss their structure to a near-spherical nanoparticles induced by potential cycling up to 1.2 V/RHE for 4000 cycles. Our previous work has demonstrated that the shape of Pt nanocubes (NCs) prepared by PVP mainly retains after potential cycling even up to 1.4 V/RHE for 200 cycles in acidic media.[25] This observation re-enforces the fact that residuals of capping agents may pre-determine the stability of shape-controlled Pt nanoparticles. Comparative study of distinctly different capping agents, PVP and oleylamine in respect to their ORR activity and shape stability under similar electrochemical conditions has not yet been reported to date. Detail knowledge helps to improve structural and electrochemical robustness of Pt NCs under fuel cell conditions.

In this work, we have investigated the effect of organic capping agents like PVP and OAm on the electrochemical ORR activities and shape durability of Pt NCs. We employed several characterization techniques like TEM, XPS, TGA and FTIR to establish the monodispersity and purity of the NCs. We compared the ORR activities of Pt NCs synthesized by PVP and OAm in different acidic electrolytes. Based on the electrochemical durability results, we have developed a degradation model for Pt NCs as a function of electrochemical parameters such upper potential and number of cycles.

Experimental Part

Materials

Dihydrogen hexachloroplatinate ($H_2PtCl_6 \cdot 6\ H_2O$, 99.9% trace metal basis, Alfa Aesar), platinum(II)acetylacetonate ($Pt(acac)_2$, 97%, Alfa Aesar), oleylamine (OAm, C18, 80–90%, Acros Organics), oleic acid (90%, Acros Organics), polyvinylpyrrolidone (PVP, Mw = 30,000, Sigma Aldrich), tungsten hexacarbonyl ($W(CO)_6$, 99.99%), silver nitrate ($AgNO_3$, 99.999% trace metal basis, Sigma Aldrich), and ethylene glycol (EG, 99.8%, Sigma Aldrich) were used without further purification.

Synthesis of PVP- and OAm-Capped Pt NCs

Details of the synthesis of PVP-capped Pt NCs have recently been reported in our previous works.[22,25,35] The original synthetic recipe from Song et al.[19] has slightly been modified as follows: All solutions were previously bubbled with Ar for at least 30 min. 3 mL of ethylene glycol (EG) was refluxed at 180 °C using an oil bath. 0.5 mL of 2 mM $AgNO_3$ was added to the boiling EG solution and heated for 5 min. Then, a mixture of 0.4 M PVP and 0.0625 M $H_2PtCl_6 \cdot 6H_2O$ (total volume of 150 μL) in EG was injected drop-wise to the hot $AgNO_3$/EG solution every 30 s over 16-min period. The rapid color change of the reaction solution from yellow-orange to dark-brown indicated the formation of colloidal Pt nanoparticles. After the last injection, the reaction mixture was heated for additional 5 min and cooled down quickly to room temperature. The final product was then ultra-sonicated and centrifuged (7.815xg/7890 revolutions per min) for 5 min and washed three times in a mixture of methanol and ethanol (volume ratio of 3:1). For the immobilization on a carbon support, 19 mg of Pt NC dispersion in 5 mL ethanol was added to 94 mg of commercial Vulcan XC72R (Cabot Corporation, US) suspended in 5 mL of ethanol. The suspension was subsequently ultra-sonicated at 40 °C for 1 h, stirred vigorously at room temperature for 48 h and finally dried at 80 °C overnight.

OAm-capped Pt NCs were prepared by a synthetic recipe reported by Sun et al.[36] A mixture of 20 mg $Pt(acac)_2$, 8 mL oleylamine, and 2 mL oleic acid was bubbled with Ar for 30 min and then heated up to 200 °C for 30 min under reflux. After quick addition of 50 mg of $W(CO)_6$ into the reaction solution under vigorous stirring, the temperature of the oil bath was further increased up to 300 °C and held then for 30 min. The obtained Pt NCs were isolated by centrifugation (7.815xg/7890 revolutions per min) for 5 min, washed in hexane for three times and finally re-dispersed in 5 mL of hexane. 5 mL of Pt NC-containing suspension was added to 45 mg of commercial Ketjen Black EC300 J (Akzo Nobel, Netherland), ultra-sonicated at 40 °C for 1 h and stirred at room temperature for 48 h. Based on our previous experiments, a good particle dispersion could be achieved by using an high surface area carbon like Ketjen Black. Afterwards, the suspension was dried at 80 °C overnight, resulting in flaky catalyst powder.

General Physical Characterization of Pt NCs

The mono-dispersity and mean particle size of as-synthesized Pt NCs were investigated using a JOEL JEM 2100F high-resolution transmission electron microscope (HR TEM) operated at 200 kV. The Pt NCs were first dispersed in ethanol and dropped onto a carbon-coated Cu mesh. All TEM micrographs were analyzed by ImageJ Software (version 1.38). The chemical composition and purity of pristine Pt NCs were established using a scanning electron microscope (SEM) equipped with an energy dispersive X-ray spectroscopy (EDX) detector (INCA, Oxford Instruments) by analyzing the characteristic energy intensities of L_α-lines for Ag, W and Pt, respectively, on several sample areas of the NC-containing films. A sample film was prepared by dropping a dispersion of Pt NCs in 100 μL of ethanol/water (1:1) on an Au-covered glass surface and dried in air. X-ray photoelectron spectroscopy (XPS) was performed on an ESCALAB 250 Xi spectrometer (Thermo Fisher) with a monochromatized Al K_α (1486.68 eV) radiation. The high-resolution XPS spectra of Pt 4f were measured at a pass energy of 10 eV, step-

© 2019 The Authors. Published by Wiley-VCH Verlag GmbH & Co. KGaA

size of 0.02 eV, dwell time of 5 ms, and an average of 10 scans, while the high-resolution XPS data for N 1s, Ag 3d, O 1s, C 1s, W 4f and Cl 2p were acquired at a pass energy of 20 eV, step-size of 0.02 eV, dwell time of 5 ms and an average of 10–20 scans. The XPS spectra were deconvoluted by CASA XPS Software (version 2.3.15) using a Gaussian-Lorentzian (GL) Tailing (T) line shape with a Shirley background. To analyze the crystalline phases of carbon-supported Pt NCs, a X-ray Diffractometer Empyrean (Panalytical, Netherland) operated with Cu K_α tube (1.45 Å) and a position-sensitive PIXCEL 1D detector (PSD). The X-ray diffraction (XRD) patterns were recorded in a 2θ range of 15–80° at a step size of 0.013° and holding time per step of 248 s and analyzed by using High Score Plus Software (version 4.5, Panalytical). Thermogravimetry analysis (TGA/SDTA851, Mettler-Toledo) was performed to determine the metal loading on the carbon-supported Pt NCs. About 5–10 mg of the sample powder was loaded onto a thermo-balance and raised from 30 to 850 °C at a heating rate of 10 °C min^{-1} in synthetic air (flow rate of 30 cm^3 min^{-1}). FTIR spectra of the Pt NCs between 400 and 4000 cm^{-1} at a resolution of 4 cm^{-1} and with average of 10 scans under continuous Ar flux were recorded using a Perkin Elmer 400 spectrometer. The unsupported Pt NC dispersions were previously dried, mixed with KBr powder and pressed to form a pellet with an outer diameter of 13 mm.

Electrochemical Characterization of Pt NCs by the Thin-Film Rotating Disk Electrode (RDE) Technique

Electrochemical RDE Setup

A RDE setup (PINE Research Instrumentation, US) with a home-made three-compartment electrochemical glass cell equipped with a potentiostat (VSP 300, Biologic, France) and a rotator was employed. 0.1 M $HClO_4$ and 0.1 M H_2SO_4 were used as electrolyte solution by diluting of a concentrated perchloric acid (70%, Sigma Aldrich, 99.999% trace metals basis) or sulphuric acid (95–98%, Sigma Aldrich, 99.999% trace metals basis) in highly purified water (18 MOhm cm at room temperature, Veolia Water System, Germany). The catalyst prepared as a thin film onto a glassy carbon (GC) of a RDE was used as a working electrode, a mercury-mercury sulphate electrode (AMETEK, US) as a reference electrode and a gold or Pt wire as a counter electrode, respectively. The reference electrode was connected to the working electrode *via* a Haber-Luggin capillary.

Preparation of the Thin Catalyst Film

The catalyst dispersions were prepared by mixing 9 mg of carbon-supported Pt NCs with 3.98 mL of purified water, 1 mL of 2-propanol and 20 μL of Nafion solution (5 wt.%, Sigma Aldrich). The mixture was then homogenized using a Branson 450-D horn sonicator (purchased by Heinemann GmbH) for 15 min. Afterwards, 10 μL of the dispersion was pipetted onto a cleaned GC electrode surface (geometric surface area of 0.196 cm^2) and dried at 40 °C in an oven under air, resulting in a thin homogeneous catalyst film. The GC electrodes were previously polished on 0.3 μm and then 0.05 μm alumina slurry (Buehler, Germany) using a Micro-cloth paper (Buehler, Germany) for 5 min each. The polished GC electrodes were rinsed and ultra-sonicated in purified water, 2-propanol and again in purified water for 5 min each. The theoretical Pt loading was estimated to be around 10–15 μg_{Pt} cm^{-2}(normalized to the geometric electrode surface area).

Electrochemical Experiments

First, an electrochemical cleaning process to obtain steady-state cyclic voltammetry (CV) profiles for carbon-supported PVP-capped and OAm-capped PT NCs NCs was performed by potential cycling up to 0.8 V/RHE at a scan rate of 200 mV s^{-1} for 200 cycles in Ar-saturated 0.1 M of electrolyte solution ($HClO_4$ or H_2SO_4). Afterwards, the electrolyte was exchanged and three CV profiles were recorded between 0.06 and 1.0 V/RHE at 50 mV s^{-1}. The electrochemically active Pt surface area (ECSA) was estimated from the last CV profiles by integrating the measured charge of hydrogen adsorption/desorption (0.06–0.40 V/RHE) with a double layer current correction and a pseudo-capacity of 205 μC $cm^{-2}{}_{Pt}$ by assuming a monolayer of hydrogen on a Pt(100) surface.[25,37]

Linear sweep voltammetry (LSV) was carried out to determine the catalytic ORR activities of Pt NCs supported on carbon. The ORR polarization curves were recorded by anodic sweeping of the potential from 0.06 to ~1.0 V/RHE at 5 mV s^{-1} and 1600 rpm (revolutions per minute) in O_2-saturated electrolyte solution. All potentials were *iR*-corrected and converted into the reversible hydrogen electrode (RHE) scale, respectively.

Accelerated durability measurements were conducted to investigate the structural stability of PVP-capped and OAm-capped Pt NCs by recording 2,000 potential cycles from 0.06 V/RHE to different upper potentials (1.0 and 1.2 V/RHE) at 50 mV s^{-1} in Ar-saturated 0.1 M $HClO_4$.

2. Results and Discussion

2.1. Mono-Dispersity and Particle-Size Distribution of As-Synthesized Pt NCs

PVP and oleylamine (OAm) were employed as capping agents in our synthetic recipes for the preparation of pure Pt NCs. Figure 1 displays the TEM micrographs of the representative Pt NCs prepared by PVP- and OAm-assisted synthetic methods at low and high magnifications and their corresponding particle size distributions. It is very obvious that both methods facilitate to prepare well-dispersed Pt NCs on the nano-scale. No particle aggregation was observed from the TEM micrographs, signifying a good efficiency of both capping agents used in the present work. By analyzing more than 200 nanoparticles from several TEM micrographs, the mono-dispersity and edge lengths of the obtained NCs were estimated. In our analysis, only nanoparticles with ±10% of deviation of aspect ratio have been taken into account as cubic nanoparticles. This is a strict criterion compared to other studies. The mean particle size was estimated in terms of mean edge length of as-prepared Pt NCs.

Based on the TEM analysis, we pointed out that the Pt NCs prepared by PVP and oleylamine exhibit a mono-dispersity of about 68±5 % and 82±3 %, respectively. The mean edge length of the OAm-capped Pt NCs is 9.3±1.8 nm and thus is larger than that of the PVP-capped Pt NCs (6.5±0.5 nm). Apart from the cubic particle shape, we observed tetrahedral (~9%), spherical (~13%), and irregular (~10%) nanoparticles as minor fractions using the PVP-assisted synthesis, while minor fractions from the OAm-assisted synthetic route consisted of tetrahedral (~12%) and irregular (~6%) nanoparticles. We can sum up that

© 2019 The Authors. Published by Wiley-VCH Verlag GmbH & Co. KGaA

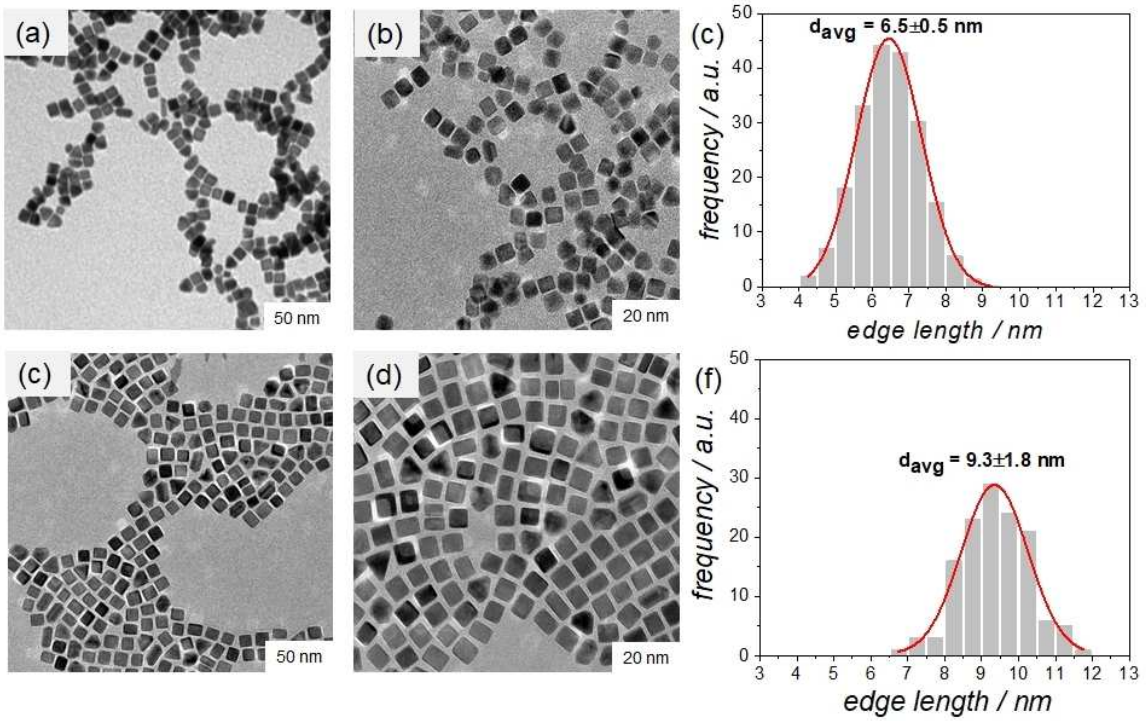

Figure 1. Low (a, d) and high (b, e) magnification HR TEM micrographs of Pt NCs prepared by PVP (top) and oleylamine (bottom) as capping agents and the respective particle size distributions (c, f).

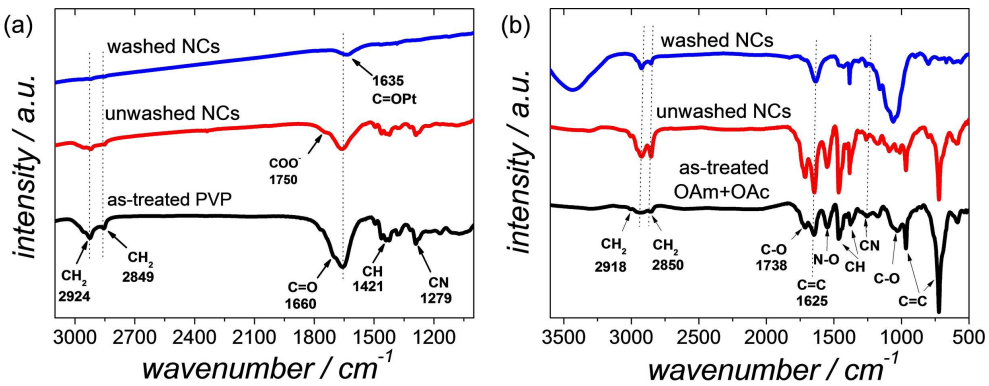

Figure 2. Series of FTIR spectra for unwashed and washed Pt NCs prepared by (a) PVP and (b) oleylamine including the reference materials like as-treated PVP and as-treated mixture of oleic acid and oleylamine. The dashed lines are indicative (a) absorption bands of C=O and CH/CH_2 for the PVP-capped Pt NCs and (b) absorption bands of CN, C=C, CH/CH_2 for the OAm-capped Pt NCs, respectively.

the OAm-assisted approach produces larger Pt NCs with improved mono-dispersity compared to the PVP-assisted.

2.2. Interactions Between Capping Agents and Pt NCs

To understand the nature of chemical/electronic interactions between capping agents and Pt NCs, we performed FTIR and XPS investigations. Figure 2 shows a series of FTIR spectra of PVP- and OAm-capped Pt NCs before and after washing. As reference spectra, as-treated PVP, oleic acid, and oleylamine were taken, respectively.

First, we will start to describe the FT-IR spectrum of as-treated PVP, where the CH stretching modes could be assigned as follows: asymmetric CH_2 stretching (methylene: 2988 cm^{-1}, pyrrolidone: 2956 cm^{-1}), symmetric CH_2 stretching (methylene: 2925 cm^{-1}; pyrrolidone: 2874 cm^{-1}), and ternary CH (2856 cm^{-1}). The absorption bands at 1400–1470 cm^{-1} correspond to the CH deformation modes from the CH_2 groups. In addition, the absorption bands at 1279 cm^{-1} and 1660 cm^{-1} are related to the C–N bending vibration and C=O stretching vibration, respectively. Both C–N and C=O stretching vibrations originate from the pyrrolidone structure of PVP. The assignment of the

© 2019 The Authors. Published by Wiley-VCH Verlag GmbH & Co. KGaA

absorption peaks of pure PVP has already been reported in our previous work.[22,35]

In case of the unwashed Pt NCs, the weak absorption band at 1750 cm^{-1} was identified as carboxylic acid (see Figure 2a), formed by hydrolysis of PVP in boiling EG. Only after washing of NCs in methanol-ethanol, the band intensity of the C=O could strongly be reduced, indicating the successful remove of weakly adsorbed PVP from the particle surface. However, the weak absorption bands such as C=O and CH_2/CH still signify the presence of strongly chemisorbed PVP residues on the particle surface. It is noted that the as-treated PVP shows a C=O stretching band at 1660 cm^{-1} compared to the pure PVP (1638 cm^{-1})[22] and washed Pt NCs (1635 cm^{-1}).The observed blue shift signifies a modification of PVP heat-treated in EG due protonation or resonance stabilization. Very importantly, for the washed NCs a shift of the carbonyl band to lower wavenumbers (red shift) is detected which is very likely attributed to the coordination of the PVP to the Pt by decrease of the electronic density in the C=O group.[38]

Figure 2b displays the FTIR spectra of unwashed and washed Pt NCs prepared by OAm-assisted synthesis. The as-treated mixture of oleic acid and oleylamine, which had previously been boiled under similar conditions but without the addition of Pt precursor and $W(CO)_6$, is taken as a reference. It is noted that the typical characteristic modes of oleyl groups from both treated oleylamine and oleic acid appear in the FTIR reference spectra: symmetric CH_2 stretching modes (methylene: 2851–2853 cm^{-1}), asymmetric CH_2 stretching modes (methylene: 2922–2925 cm^{-1}), deformation mode of NH_2 group at 1625 cm^{-1} and CH deformation of cis-disubstituted alkenes at 720 cm^{-1}. The additional mode at 1738 cm^{-1} is characteristic for the carboxylic acid group of oleic acid, while a weak peak at 1538 cm^{-1} could be assigned to the mode of υ(-CN) from the oleylamine. Further assignments of amine groups (especially primary amine) are very difficult in the FTIR spectrum due to the overlap of broad absorption bands of OH groups in the range of 3200–3500 cm^{-1}.

For the unwashed Pt NCs the characteristic absorption bands from CH_2 and C=C groups are clearly visible in the FTIR spectrum (see Figure 2b). It is obvious that the FTIR spectrum of the unwashed Pt NCs resembles that of the treated oleylamine and oleic acid. After washing, only few absorption bands with lower intensities appear in the FTIR spectrum of the washed Pt NCs due to the successful cleaning step. Due to superimposition with bands from solvent/moisture residues, a clear discrimination of oleic acid and oleylamine, yet, seems to be unfeasible and thus the question of which compound act as capping agent for the NC synthesis could not be addressed only by FTIR.

Moreover, electronic interactions between capping agents and Pt NCs were also investigated by XPS, where particle ensembles were prepared as dried film on an Au-covered glass substrate. Definitely, both XPS survey spectra of the obtained NCs exhibit the presence of C, O and N species apart from Pt (not shown). The C 1s and O 1s XPS spectra were not considered for analysis because solvent residuals like hexane and/or methanol/ethanol could remain in the washed samples. Very interestingly, the XPS spectra of both washed Pt NCs show the appearance of nitrogen species (see Figure 3) which can only come from the capping agents like PVP and oleylamine. The N 1s XPS signals of as-treated PVP and oleylamine/oleic acid were used as references. In Figure 3a, for the washed Pt NCs the binding energy of the large N 1s XPS signal at 399.8 eV is similar to that of the as-treated PVP (399.7 eV), indicating the presence of weakly adsorbed PVP on the particle surface. More interestingly, a smaller N 1s signal shifted to lower binding energy appears in the XPS spectrum of the washed Pt NCs. This signal is associated with the chemisorbed PVP, where the pyrrolidone ring of the chemisorbed PVP interacts strongly with the Pt surface. Similar observation has been reported for PVP-capped spherical and cubic Pt nanoparticles, where systematic XPS investigations were performed to provide information about the electronic donator-acceptor interactions between PVP and Pt surface ranging from nanoparticles to polycrystalline bulk materials.[39].

In Figure 3b, the as-treated oleylamine/oleic acid shows two different nitrogen species in the high-resolution N 1s XPS spectrum. We assume that the N 1s XPS signal at 399.7 eV corresponds to the oleylamine, while the N 1s XPS peak shifted to higher binding energies at 401.5 eV may be related carboxylate derivatives (interaction between oleylamine and oleic acid). In addition, the intensity of the N 1s XPS signal is very low for washed NCs due to the effective solvent washing process. Interestingly, the binding energies of the N 1s for washed NCs is quite similar those for treated oleylamine/oleic. This observation indicates a weak capping behavior of oleylamine on the Pt surface. It is noted that oleic acid does not contain nitrogen atoms in its structure and thus we point out that oleylamine acts as capping agent. This result reveals the remarkable role of oleylamine as capping agent during the preparation of Pt NCs.

2.3. Structural and Compositional Analysis of Pt NCs via XRD, EDX, and XPS

Pt NCs were fabricated using Ag^+ ions and $W(CO)_6$ in the PVP- and OAm-assisted synthetic routes, respectively. The question about the purity of the obtained NCs often arises and if silver or tungsten is incorporated into the Pt lattice to form an alloy, for instance. To address this point, various characterization techniques like XRD, EDX, and XPS were employed in this work.

XRD profiles of the PVP- (black line) and OAm-capped Pt NCs (blue line) supported on carbon are shown in Figure S1 (supplementary information). The reflexes at 2θ values of 39.7, 46.3, and 67.4° are assigned to the (100), (200), and (220) lattice planes of face-centered cubic (fcc) Pt structure (space group of Fm-3 m). Although the broadening of reflexes for nanocrystallite sizes makes the XRD interpretation difficult, the reflexes do not show any shift in respect to the pure Pt lattice, indicating that the Ag or W is not inserted in the Pt NCs. No additional reflexes based on Ag- or W-containing crystal phases were observed in the XRD profiles. Moreover, the chemical composition of particle ensembles as a dried film on a freshly Au-covered glass substrate was investigated using SEM-EDX and XPS technique. Our EDX analysis reveals that the PVP-capped NCs consist of about 99 at.% of Pt and less than 1 at.% of Ag, while about 95 at.% of Pt and 5 at.% of W was

© 2019 The Authors. Published by Wiley-VCH Verlag GmbH & Co. KGaA

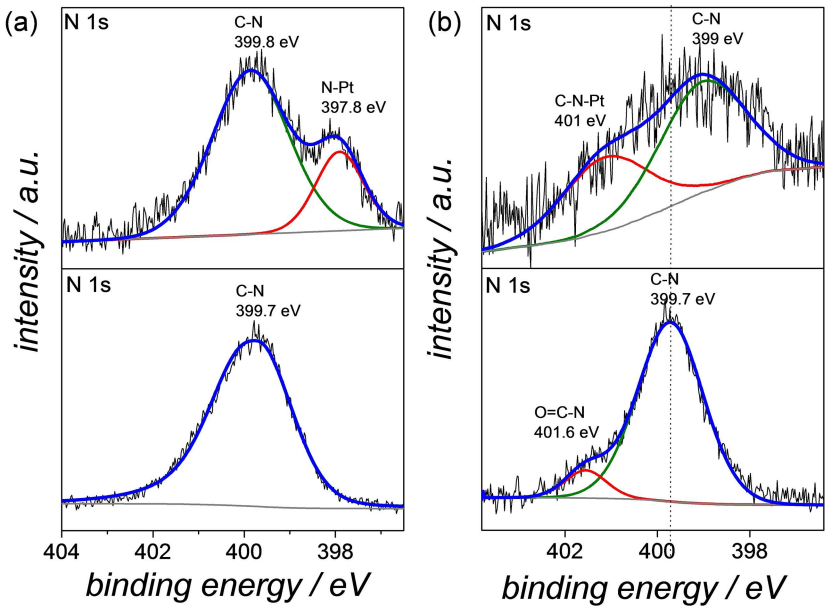

Figure 3. High-resolution N 1s XPS spectra of (a, top) PVP-capped Pt NCs and (b, top) OAm-capped Pt NCs after washing. The as-treated PVP (a, bottom) and as-treated oleylamine/oleic acid (b, bottom) are shown as reference. Grey line indicates the background, the components are shown in red and green lines and the sum curve is illustrated as a solid blue line, respectively.

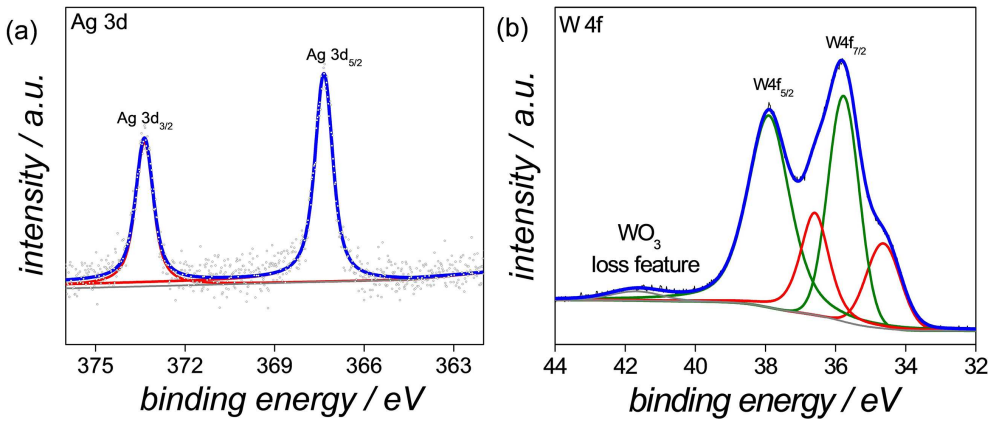

Figure 4. High-resolution XPS spectra of (a) Ag 3d for the PVP-capped Pt NCs and (b) W 4f for the OAm-capped Pt NCs. Grey line indicates the background, the components are shown in red and green lines and the sum curve is illustrated as a solid blue line.

determined for the OAm-capped NCs. This result reveals that the silver is almost removed after synthesis, whereby tungsten remains at low content in the Pt NCs.

Now we focus on the chemical states of Ag and W residuals used as additives for the synthesis of NCs. Figure 4 displays the high-resolution XPS spectra of Ag 3d and W 4f for the PVP- and OAm-capped Pt NC-containing films, respectively. As reference, the metallic silver (Ag^0) exhibits a binding energy of Ag $3d_{5/2}$ at 368.2 eV.[35,40] In our case, the binding energy of the Ag $3d_{5/2}$ peak is clearly shifted to 367.3 eV and the peak appears symmetric which may be attributed to the presence of oxidized Ag. Very low content of Cl^- was found in the XPS survey spectrum, indicating that the silver might appear not only as oxides but also as silver chloride.

The high-resolution W 4f XPS spectrum clearly signifies several oxidation states of tungsten in the OAm-capped Pt NC sample. The W 4f core level spectrum was deconvoluted with two spin-orbit doublets corresponding to two different oxidation states of W. The W $4f_{7/2}$ and W $4f_{5/2}$ peaks at 35.7 and 37.8 eV, respectively, can be attributed to the oxidation state of W^{6+} (reference binding energies: $W^0 = 31.2$ eV, $W^{4+} = 32.9$ eV and $W^{6+} = 35.8$ eV[41–43]). The second doublet at lower values of binding energy of 34.6 and 36.6 eV arises due to emissions from W $4f_{7/2}$ and W $4f_{5/2}$ core levels, respectively, corresponding to the presence of W^{5+}. A loss feature for WO_3 appears at 41.8 eV. Based on the XPS analysis, we sum up that both Ag and W residues exist largely as oxides and/or chlorides. These by-products can easily be removed by extensive washing to

© 2019 The Authors. Published by Wiley-VCH Verlag GmbH & Co. KGaA

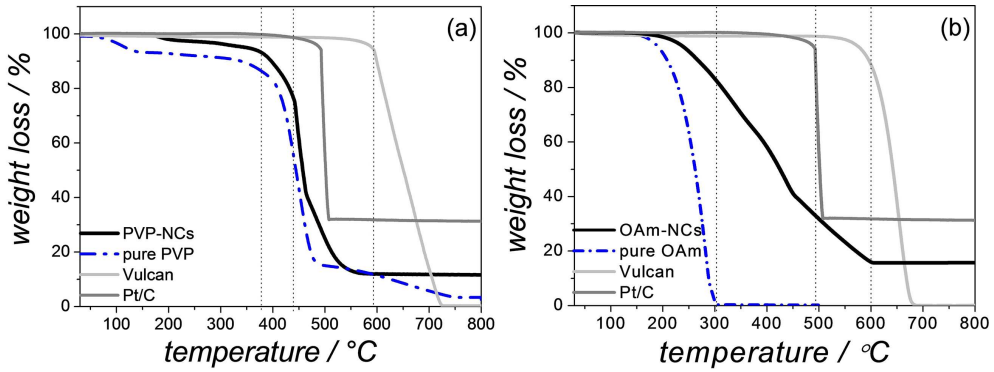

Figure 5. Thermogravimetric (TG) profiles of (a) PVP-capped Pt NCs and (b) OAm-capped Pt NCs denoted as black lines under synthetic air environment (flow rate of 30 sccm and at 20 °C min^{-1}). Reference G profiles of pure capping agents (in blue dashed lines), pure carbon (in light grey) and comm. Pt/C (in dark grey) are shown for comparison. The dashed black lines indicate the different decomposition regions of PVP- and OAm-capped Pt NCs, respectively.

produce highly mono-dispersive and pure Pt NCs using both synthetic routes.

2.4. Thermogravimetric (TG) Analysis of Carbon-Supported Pt NCs

TG measurements were carried out to determine the actual metal loading for Pt NCs supported on carbon and very likely to provide information of residuals of capping agents on the particle surface.

Figure 5 shows the TG profiles of both carbon-supported Pt NCs prepared by PVP- and OAm-assisted synthetic routes. It is obvious that the TG profiles of the PVP- and OAm-capped NCs show a very complex degradation behavior including several oxidation processes under synthetic air atmosphere. To better understand the temperature-controlled decomposition characteristics of the PVP- and OAm-capped Pt NCs, we evaluated the thermal decomposition behavior of pure capping agents (PVP and OAm), pure carbons (Vulcan and Ketjen Black) and commercial Pt/C (28 wt.%) as reference materials. First, we will discuss the TG curves of pure carbons (Vulcan, Ketjen Black). As mentioned above, the PVP-capped Pt NCs were deposited on Vulcan, while Ketjen Black was used for the OAm-capped Pt NCs to obtain a good quality of particle dispersion which is highly critical for later electrochemical investigations (see chapter 2.5). We suggest that the improved dispersion of OAm-capped Pt NCs on a high surface area carbon is very likely based on its larger particle size. Figure 5 shows a simple degradation behavior of both carbons starting around ~500 °C up to 710 °C under synthetic air atmosphere, which is expected for carbon gasification processes. A faster oxidative decomposition of Ketjen Black (below 700 °C) was observed compared to that for Vulcan due to its less degree of graphitization.

Moreover, the TG profile of pure PVP shows multi-step processes of decomposition in synthetic air. The first decomposition process seems to be between 100 and 400 °C, indicating the volatilization of loosely-bound alkyl chains and monomers at lower temperatures. Further decomposition processes are to find from 400 to 700 °C, whereby at temperatures higher than 500 °C the release of the pyrrolidone groups occur as reported in other works.[25,44] Very interestingly, we observed similar degradation behavior in the TG profile of PVP-capped NCs (black curve), signifying the presence of adsorbed PVP on the Pt surface in spite of washing. We want to stress that the degradative steps are more pronounced by using pure oxygen to decompose the adsorbed PVP on the Pt surface as shown in our previous work.[25] Finally, above 600 °C the PVP residues and carbon are entirely oxidized and the remaining platinum was found to be around 11 wt.%.

The TG profile of pure oleylamine is represented in Figure 5b (blue curve), revealing that its evaporation takes place between 190 and 300 °C which is in agreement with literature.[45] The boiling point of oleylamine is around 145 °C. The TG profile of the OAm-capped Pt NCs recorded in synthetic air shows at least three dominant processes of decomposition from 200–380 °C, 380–450 °C, and 450–600 °C, respectively. Humphrey et al.[46] have reported the degradation of OAm-capped Pt/C *via* two stages using TGA-MS: the cleavage of C=C to form shorter alkyl fragments and subsequently by degradation of amine and longer alkyl fragments at higher temperatures. Based on their study, we suggest that the first decomposition processes of the oleylamine are very likely related to the release of shorter hydrocarbon fractions at lower temperatures followed by longer hydrocarbon and amine fractions up to 450 °C and finally the oxidation of carbon support material at higher temperatures. After the total decomposition of residual OAm and carbon, the remaining Pt content was estimated to be 16 wt.%. Based on the TG results, we can sum up that the thermal decomposition profiles of washed Pt NCs prepared by both recipes indicates the presence of residuals of capping agents which is in good agreement with the XPS and FTIR data (see Figure 3 and Figure 4).

© 2019 The Authors. Published by Wiley-VCH Verlag GmbH & Co. KGaA

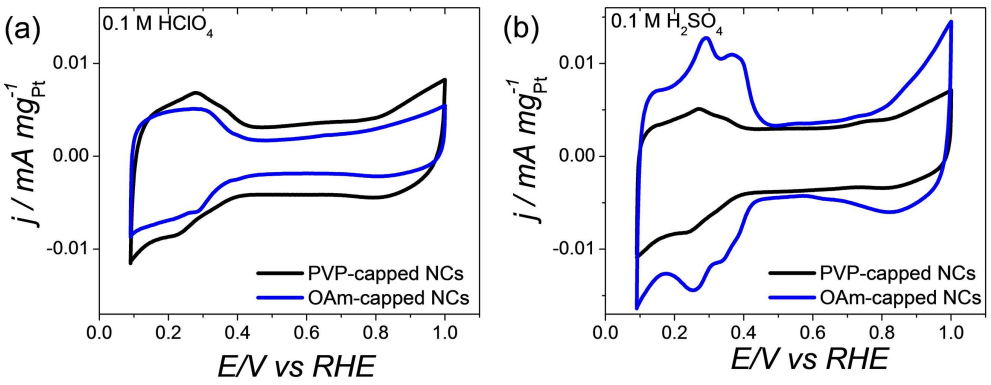

Figure 6. CV profiles of the PVP- and OAm-capped Pt NCs in 0.1 M Ar-saturated (a) $HClO_4$ and (b) H_2SO_4. Experimental parameters: Pt loading of 10–15 μg cm^{-2}, scan rate of 50 mV s^{-1}.

2.5. Electrochemical Characterization of Pt NCs

The electrochemical behaviors of carbon-supported Pt NCs prepared by PVP and oleylamine were studied by recording of cyclic voltammetry (CV) profiles in Ar-saturated 0.1 M $HClO_4$ and 0.1 M H_2SO_4. Based on the TEM results (not shown), good particle dispersion and similar Pt loadings have been achieved if the PVP-capped Pt NCs are deposited on Vulcan and the OAm-capped NCs on Ketjen Black. Unfortunately, using the same carbon support does not produce well isolated Pt NCs with similar metal loading. Because the quality of dispersion has a strong influence on the catalytic performance for electrochemical oxygen reduction reaction (ORR), we decided to study the as-prepared Pt NCs supported on different carbon materials.

Figure 6a shows the CV profiles of the electrochemically cleaned PVP- and OAm-capped Pt NCs in 0.1 M $HClO_4$. In principle, the CV profiles of Pt NCs are very similar to that of a commercial Pt/C, but with some important differences which will be discussed now. Typically, the CV profile of a clean Pt surface shows characteristic voltammetric features relating to the hydrogen ad-/desorption regime (underpotentially deposited hydrogen, Hupd, 0.06–0.4 V/RHE), double layer region (0.4–0.6 V/RHE) and formation/reduction of Pt (hydro)oxide (above 0.6 V/RHE), respectively. It is obvious that for both PVP- and OAm-capped NCs the electrochemical features in the Hupd region are clearly visible, signifying the accessibility and utilization of the particle surface. However, on closer inspection the formation and reduction of Pt (hydr)oxide at higher anodic potentials are not well pronounced, indicating the presence of site-blockage species like PVP and OAm on the NC surface. Generally, the ad-/desorption processes of capping agents are very likely controlled by applied potential, which modifies the surface charge of the electrode (electronic interactions). Compared to the OAm-capped Pt NCs, an increased current density in the electric double layer region for the PVP-capped is found, which is very likely attributed to lower Pt loading, capacity current of different carbon support, and/or PVP residuals.

Due to the strong adsorption of (bi)sulphate anions on the Pt surface, the electrochemical features in respect to the surface orientation like Pt(100) are very sensitive and more pronounced in sulphuric acid compared to those in perchloric acid (weakly adsorbed anions). Therefore, we employed 0.1 M H_2SO_4 as electrolyte solution to expose the electrochemical features of a Pt(100) surface which are present in ideal cubic nanoparticles. Figure 6b displays the CV profiles of PVP- and OAm-capped Pt NCs in 0.1 M H_2SO_4. First, the CV profile of the PVP-capped NCs shows similar Hupd features in 0.1 M H_2SO_4 compared to those in 0.1 M $HClO_4$. Unlike, for the OAm-capped Pt NCs the Hupd region shows clearly current peaks at 0.28 and 0.37 V/RHE, which are assigned to the Pt(100)-preferential surface structure.[47,48] Particularly, the broad current peak at 0.37 V/RHE is a characteristic feature of Pt(100) terraces as reported by Clavilier et al.[48] Altogether, we point out that the exposure of the current peaks related to Pt(100) terraces reveals a weak adsorption behavior of oleylamine on the particle surface compared to that for PVP.

In order to evaluate the electrochemically active surface area (ECSA) of the obtained Pt NCs, we used the mean integral charge of the Hupd region with double layer correction and by normalizing with the initial metal mass of the catalyst used and with the pseudo-capacity of 205 μC cm^{-2} for a single Pt(100) crystal.[25,37] In this work, a commercial 28 wt.% Pt/C (TEC10 V30E, Tanaka/Japan) as benchmark fuel cell catalyst was taken. Table 1 shows the ECSA values of the PVP-capped Pt NCs (mean particle size of 6–7 nm), OAm-capped Pt NCs (9–10 nm) and commercial Pt/C (2–3 nm) in $HClO_4$ and H_2SO_4, respectively.

Table 1. ECSA and ORR activities (SA and MA) of the PVP- and OAm-capped Pt NCs and commercial Pt/C (TEC10 V30E, Tanaka/Japan) in 0.1 M $HClO_4$ determined from five independent measurements. The electrochemical results in 0.1 M H_2SO_4 are given in round brackets. Mean particle sizes were estimated from the TEM data.

	Particle size [nm] *via* TEM	ECSA [$m^2 g_{Pt}^{-1}$]	SA [$\mu A\,cm_{Pt}^{-2}$]	MA [$A\,mg_{Pt}^{-1}$]
TKK–Pt/C	2.3 ± 0.6	73 ± 5 (63 ± 4)	206 ± 22 (162 ± 3)	0.14 ± 0.02 (0.10 ± 0.02)
OAm–Pt NCs	9.3 ± 1.8	56 ± 3 (45 ± 6)	398 ± 8 (164 ± 9)	0.22 ± 0.02 (0.11 ± 0.01)
PVP–Pt NCs	6.5 ± 0.5	30 ± 2 (23 ± 2)	179 ± 6 (128 ± 5)	0.03 ± 0.01 (0.03 ± 0.01)

© 2019 The Authors. Published by Wiley-VCH Verlag GmbH & Co. KGaA

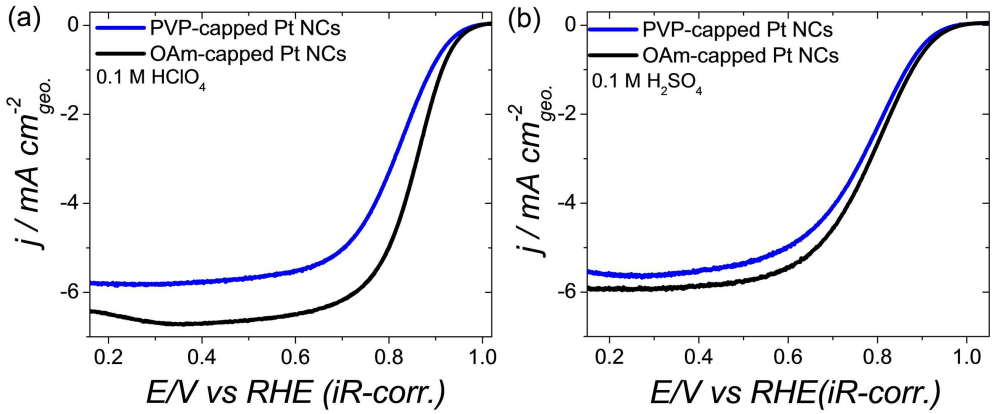

Figure 7. ORR polarization curves of PVP-capped and OAm-capped Pt NCs in O_2-saturated (a) 0.1 M $HClO_4$ and (b) 0.1 M H_2SO_4. Experimental parameters: anodic scan from 0.06–1.0 V/RHE at 5 mV s^{-1} and 1600 rpm; Pt loading of 10–15 μg cm^{-2}.

First, we observed that the ECSA values are lower in 0.1 M H_2SO_4 compared to those in 0.1 M $HClO_4$ due to the strong adsorption behavior of (bi)sulphate anions on the Pt surface. Secondly, the ECSA values in 0.1 M $HClO_4$ increase accordingly: PVP-capped Pt NCs (30 ± 2 $m^2 g_{Pt}^{-1}$) < OAm-capped Pt NCs (56 ± 3 $m^2 g_{Pt}^{-1}$) < Pt/C (73 ± 5 $m^2 g_{Pt}^{-1}$). A similar trend was observed in sulphuric acid. To evaluate the various particle shapes and particle sizes, we estimated the surface area-to-volume ratio as an indicator for the utilization of Pt surface atoms. It is expected that the surface area-to-volume ratio decreases in the order: commercial Pt (2.4) > PVP-capped NCs (0.9) > OAm-capped Pt NCs (0.6). Thus, the spherical Pt nanoparticles show a higher surface area-to-volume ratio by a factor of at least two compared to the NCs. Very remarkable, despite larger particle size and thus lower surface area-to-volume ratio the OAm-capped Pt NCs exhibit a higher ECSA value than the PVP-capped. This observation confirmed the moderate capping properties of the oleylamine compared to that for PVP.

2.6. Oxygen Reduction Reaction (ORR) Activities of Pt NCs

One of the critical parameters used to determine the ORR performance of electrocatalysts is the Pt surface area-based specific activity (SA) (reflects the number of catalytically active sites) and Pt mass-based activity (MA). Figure 7 shows the ORR polarization curves of Pt NCs in O_2-saturated 0.1 M $HClO_4$ and H_2SO_4. All polarization curves exhibit a plateau-like behavior between 0.06–0.6 V/RHE, indicating the mass transport limiting current density for ORR. In this region, diffusion of reacting species towards the electrode surface dominates over the reaction kinetics. The onset potential from the mass-transport limiting region to the mixed kinetic-mass transport controlled region takes place at ~0.7 V/RHE. Above 0.85 V/RHE the current density solely originates from the ORR kinetics of the Pt NCs and is thus independent on the rotation speed of the electrode.

Table 1 displays a summary of the SA and MA for PVP- and OAm-capped Pt NCs at 0.9 V (iR-corrected) in O_2-saturated 0.1 M $HClO_4$ and H_2SO_4. As expected, the SA and MA are mainly lower in H_2SO_4 based on the blockage of strongly adsorbed (bi) sulphate anions. Very interestingly, the OAm-capped Pt NCs show an increase of the SA by a factor of 2–3 compared to the PVP-capped Pt NCs and commercial Pt/C, while its MA is very similar to the Pt/C and around 7 times higher than that for the PVP-capped. This result is very remarkable because the mean particle size of the OAm-capped Pt NCs is around 10 nm and therefore much larger than that for the Pt/C (2–3 nm). Despite intensive washing and electrochemical cleaning, the PVP-capped Pt NCs show a similar SA but very low MA compared to the Pt/C. The insufficient ORR performance of the PVP-capped NCs is attributed to the strong adsorption behavior of PVP which hinders the accessibility to the catalytically active Pt sites. Therefore, further treatment methods for the PVP-capped NCs are required to entirely remove the polymer from the particle surface, while the NCs prepared by oleylamine can directly be applied as ORR electrocatalyst.

2.7. Accelerated Stress Test Protocol of Pt NCs

Structural stability and long-term performance have become a major importance in the development of shape-controlled Pt-based nanoparticles. To investigate the particle shape stability and durability of Pt NCs in electrochemical environments, we performed an accelerated stress test (AST) protocol by recording up to 2,000 potential cycles with a scan rate of 50 mV s^{-1} between 0.06–1.0 V/RHE and 0.06–1.2 V/RHE in Ar-saturated 0.1 M $HClO_4$.

The results from the electrochemical cycling up to 1.0 V/RHE for PVP- and OAm-capped Pt NCs are illustrated in Figure S2 (see supporting information). In case of the PVP-capped NCs, the current density in the Hupd regime is successively decreased with increasing cycle number, signifying a loss of ECSA *via* particle detachment, changes of surface arrangement (loss of particle shape) and/or modification in adsorption behavior of electrochemically treated PVP. In addition, the electrochemical features for Pt (hydr)oxide formation are less pronounced during the entire run, indicating a strong blockage

© 2019 The Authors. Published by Wiley-VCH Verlag GmbH & Co. KGaA

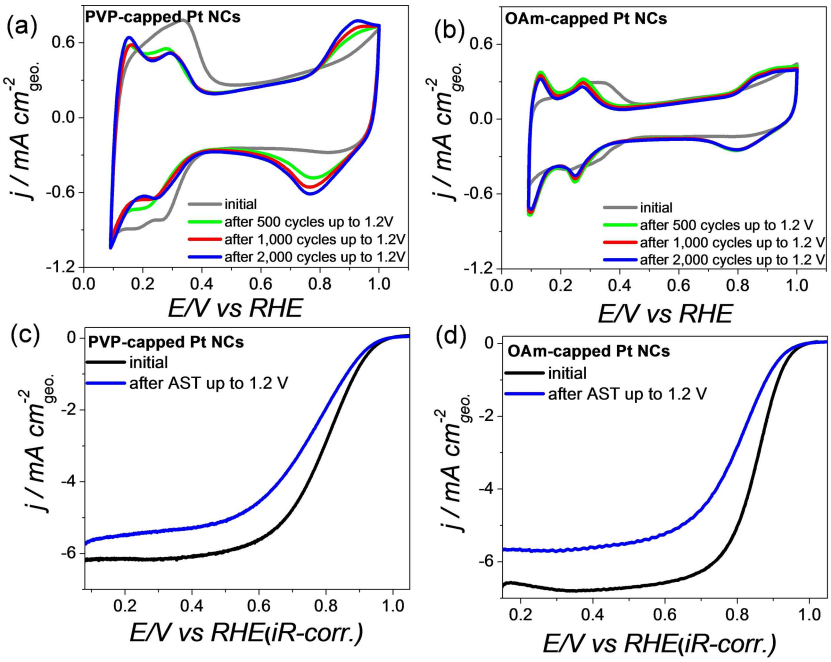

Figure 8. CV profiles and ORR polarization curves of (a, c) PVP-capped Pt NCs and (b, d) OAm-capped NCs Pt before and after the accelerated stress protocol (2,000 cycles, between 0.06 and 1.2 V/RHE at 50 mV s^{-1}) in 0.1 M $HClO_4$.

behavior of PVP polymer on the Pt NCs at potentials up to 1.0 V/RHE. Unlike, the OAm-capped Pt NCs show drastic changes in electrochemical features in the Hupd and Pt (hydr) oxide regimes during the first 500 cycles. Afterwards, the CV profiles for the OAm-capped NCs are unchanged. Generally, the electrochemical features in the Hupd region correlate with different adsorption energies of hydrogen on a specific surface orientation and structure.

Doubtlessly, the aging processes for both Pt NC catalysts are more accelerated by increasing the upper potential. Figure 8a-b display the changes in CV profiles for Pt NCs prepared by PVP- and OAm-assisted route after 500, 1,000, and 2,000 potential cycles between 0.06–1.2 V/RHE. For the PVP-capped Pt NCs, the electrochemical features of Pt (hydr)oxide formation/reduction are exposed after 500 cycles up to 1.2 V/RHE, indicating a further cleaning process of the particle surface, e.g. by electrochemical oxidation of PVP. It is noted that the evolution of distinct current peaks in the Hupd regime is associated with the changes in surface arrangement and structure of PVP-capped Pt NCs. These pronounced current peaks between 0.06–0.4 V/RHE are very likely caused by surface restructuring and/or re-adsorption of oxidized PVP from the electrolyte solution.

Figure 8b displays the cycle number-resolved changes in CV profiles for OAm-capped NCs between 0.06 and 1.2 V/RHE. It is noted that the changes in the Hupd region for OAm-capped Pt NCs had already been occurred in the first hundred potential cycles, while several of hundreds cycles up to 1.0 V were needed to observe similar changes in the electrochemical features. More precisely, the current peaks at 0.13 and 0.28 V/RHE appeared simultaneously during the first hundred cycles, while the current peak at 0.37 V/RHE assigned to (100) terraces gradually decreased until it almost disappeared. Afterwards, the CV profiles for OAm-capped Pt NCs are almost unchanged up to 2,000 cycles. This observation highlights the fast degradation processes of OAm-capped NCs with exposed (100) facets induced by potential cycling. In other words, with increasing upper potential, the (100) terraces undergo surface restructuring by evolution of (111) and (110) surface orientations. The enhanced catalyst aging with higher upper potential is very likely related to the incorporation of oxygen in the Pt sublayers, resulting in increased surface roughness and/or the increased electrochemical oxidation of adsorbed capping agent.

Figures S2c–2d and 8c–8d display the comparison of ORR polarization curves of PVP- and OAm-capped Pt NCs before and after both accelerated stress (AST) protocols. It is obvious that the diffusion limiting currents and half wave potentials for both Pt NCs degrade during AST experiments. In other words, a significant shift of the half wave potentials to lower values signifies a drop of ORR activity especially for OAm-capped Pt NCs. Obviously, the loss of catalytic performance is strongly enhanced for OAm-capped Pt NCs compared to that for PVP-capped.

Table 2 compares the final ECSA and ORR activities for both Pt NCs after 2,000 cycles up to 1.0 and 1.2 V/RHE. It is obvious that slight changes (loss of ~10%) in ECSA and ORR activities of the PVP-capped NCs were observed after both AST protocols. Unlike, the OAm-capped NCs show significant performance losses with a drop of ECSA of about 21% and 30% after 2,000 cycles up to 1.0 and 1.2 V/RHE, respectively. Moreover, ORR activity losses of 50–60% were recorded after 2,000 cycles up to 1.0 and 1.2 V/RHE. It is noted that during the experiment the

© 2019 The Authors. Published by Wiley-VCH Verlag GmbH & Co. KGaA

Table 2. ECSA and ORR activities of PVP- and OAm-capped Pt NCs before and after electrochemical durability test (2,000 cycles up to 1.2 V/RHE) in 0.1 M $HClO_4$. SA and MA were obtained from the ORR polarization curves at 0.9 V (iR-corrected).

	After 1.0 V/RHE			After 1.2 V/RHE		
	ECSA $[m^2 g_{Pt}^{-1}]$	SA $[\mu A\, cm_{Pt}^{-2}]$	MA $[A\, mg_{Pt}^{-1}]$	ECSA $[m^2 g_{Pt}^{-1}]$	SA $[\mu A\, cm_{Pt}^{-2}]$	MA $[A\, mg_{Pt}^{-1}]$
OAm	44 ± 5	170 ± 9	0.12 ± 0.02	39 ± 5	189 ± 9	0.12 ± 0.02
PVP	24 ± 5	110 ± 5	0.02 ± 0.02	25 ± 3	182 ± 8	0.03 ± 0.01

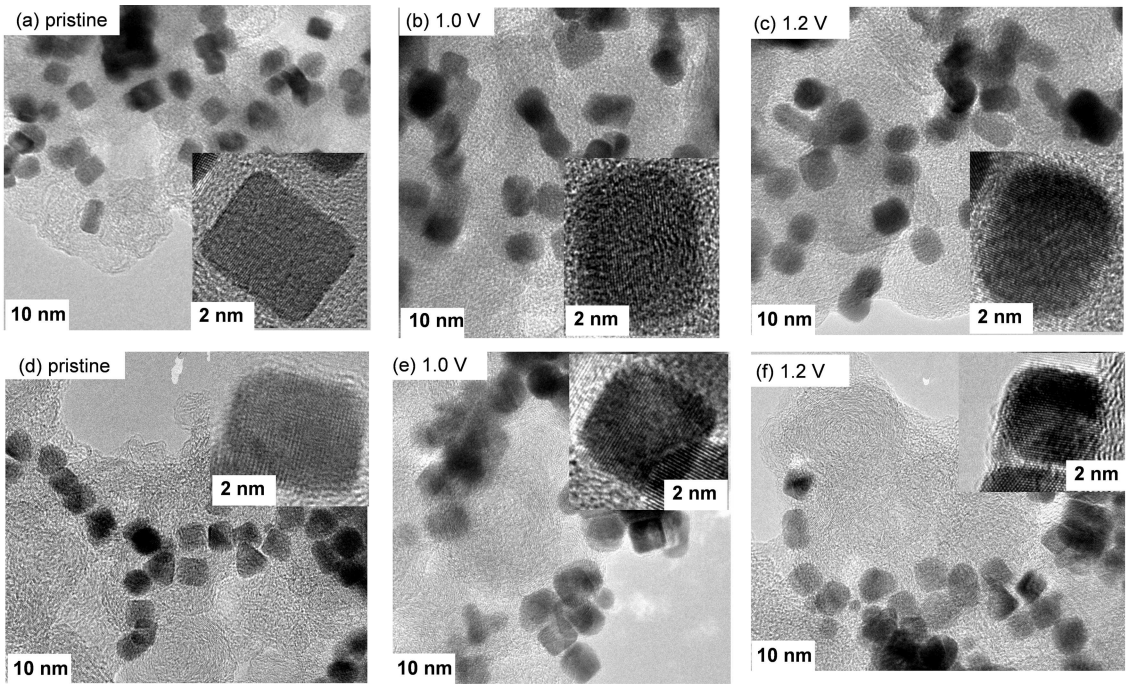

Figure 9. HR TEM micrographs of (upper part) OAm-capped NCs and (lower part) PVP-capped NCs supported on carbon before (a) and after AST protocols between (b) 0.06–1.0 V/RHE and (c) 0.06–1.2 V/RHE at 50 $mV\,s^{-1}$ in 0.1 M $HClO_4$.

upper potential had not exceeded 1.2 V/RHE and thus the carbon corrosion can mainly be neglected. The accelerated aging of OAm-capped NCs is very likely attributed to the structural changes (loss of particle shape) and/or particle detachment based on insufficient immobilization of particles. The weak immobilization of particles, however, would be noticeable during electrochemical cleaning, but a loss of ECSA was not observed and thus we can mainly exclude this point. Altogether, we can sum up that the OAm-capped Pt NCs degrade much faster compared to the PVP-capped and its performance loss strongly depends on the upper potential.

Figure 9 shows HR TEM micrographs of single Pt NCs before and after AST protocols between 0.06–1.0 V/RHE and 0.06–1.2 V/RHE to correlate the electrochemical results with structural changes in particle shapes and sizes of NCs. It is important to mention that shape analysis *via* TEM is not trivial due to particle agglomeration and poor image contrast for carbon-supported NCs. To the best of our ability, we focused on single NCs and did not take account the agglomerated NCs.

To sum up, the analysis of around 120 single OAm-capped nanoparticles reveals dramatic changes in mono-dispersity after both AST protocols. More precisely, the potential cycling up to 1.2 V/RHE leads to ~75% of near-spherical particles for OAm-capped NCs, while around 65% of rounded cubes were found after cycling up to 1.0 V (see Figure 9 a–c). Unlike, the PVP-capped samples almost retain their particle size and shape (based on the analysis of around one hundred of single nanoparticles: ~61% of nanocubes after cycling up to 1.0 V/RHE, while 56% of nanocubes up to 1.2 V, shown in Figure 9 d–f).

The structural transformation to the thermodynamically stable particle shape is consistent with the electrochemical durability studies of OAm-capped Pt NCs (with sizes of 7–8 nm) reported by Markovic et al.[21] Consequently, the exposed surface atoms (especially corner and edge atoms with lower coordination numbers) undergo surface rearrangement and/or re-structuring to reduce the total surface energy by formation of (111) terraces, resulting in the evolution of thermodynamically stable near-spherical particle shape. It is worth to mention that the diameter of the near-spherical nanoparticles was estimated to be around 11 nm, where a typical growth in particle size in respect to the similarities of the total volume between the initially cubic (edge length of 10 nm) and spherical (diameter of 11 nm) nanoparticles can almost be neglected. The

© 2019 The Authors. Published by Wiley-VCH Verlag GmbH & Co. KGaA

transformation process from cubic to spherical nanoparticles is accelerated by applying potentials higher than 1.0 V/RHE. In contrast, the structural robustness of PVP-capped NCs under accelerated aging conditions is based on the strong re-adsorption of the PVP residues. We assume that the adsorption of the strong capping agent like PVP significantly reduces the mobility of Pt surface atoms and hinders the diffusion to lower surface energy sites. This observation is in excellent agreement with our previous work, where we have reported the structural stability of PVP-capped NCs after potential cycling up to 1.4 V/RHE.[25] In principle, the strong capping nature is favorable for preservation of the cubic structure under highly corrosive conditions.

We can sum up that OAm-capped NCs have shown promising electrocatalytic activities for ORR, but the structural instability at potential above 1.0 V/RHE is still a major concern. The use of strong capping agents improves the robustness of particle shape accompanied by low catalytic performance due to the blockage effects.

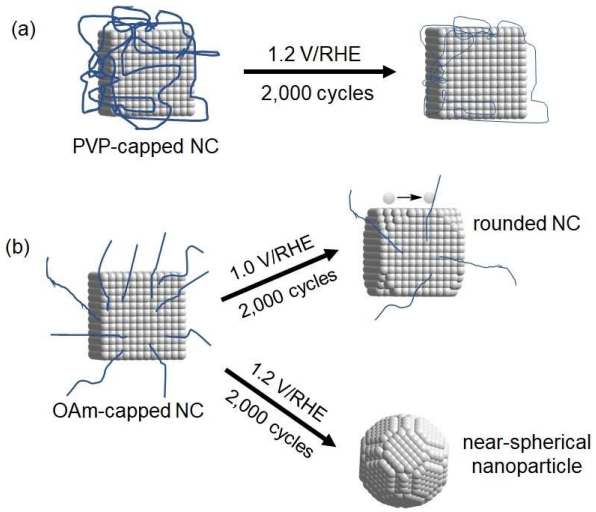

Figure 10. Shape degradation model of (a) PVP-capped Pt NCs and (b) OAm-capped Pt NCs in 0.1 M $HClO_4$ under different electrochemical conditions (1.0 and 1.2 V/RHE after 2000 cycles).

2.8. Structural Transformation Model of Shape-Controlled Nanoparticles

Based on the present work, we developed a structural transformation model of cubic nanoparticles as a promising ORR electrocatalyst under electrochemical conditions. PVP and oleylamine were applied as capping agents to fabricate mono-disperse Pt NCs with an edge length of several nanometers. Obviously, both agents exhibit distinctly different capping properties and strength. For instance, PVP is known as a polymer to strongly adsorb on the Pt surface, while oleylamine is classified as moderate capping agent. After synthesis and several washing steps, residuals of both capping agents are still found on the particle surface. Electronic interactions of PVP or oleylamine with the Pt surface could be proven by XPS, FTIR and TGA. Generally, properties of the Pt surface are strongly dependent on the capping strength, which can be described by utilization of Pt (ECSA) and electrocatalytic ORR activity of NCs. Due to its moderate adsorption properties, the OAm-capped Pt NCs show remarkable ECSA and Pt surface area-based specific and Pt mass-based ORR activities (SA and MA) compared to the PVP-capped and pure Pt/C. Although the exposure of the Pt (100) terraces for OAm-capped NCs are illustrated, the robustness of the particle shape dramatically suffers from the applied potential. If a capping agent like oleylamine is partially oxidized at high anodic potentials, the exposure of surface atoms increases more and more until a so-called "naked" Pt surface of NCs is obtained. The stage of "naked" surface can only be achieved by entire oxidation of weakly adsorbed capping agents. The clean surface exhibits a relatively high mobility of surface atoms, in particular edge and corner atoms with high surface energy. In contrast, the PVP polymer is strongly adsorbed on the metallic surface and stabilizes particularly the low coordinated surface atoms.

Figure 10 displays our structural transformation model of Pt NCs prepared by PVP- and OAm-assisted synthesis, two distinctly different capping agents, as a function of the upper potential and cycle number as critical parameters. It is noted that potentials above 1 V/RHE accelerate the structural aging associated with a significant drop of catalytic performance of NCs. In this case, the well-defined cubic nanoparticles with a "naked" surface easily transforms into a thermodynamically stable near-spherical particles after few potential cycles. The shape degradation starts with a loss of low-coordinated corner and edge atoms, which diffuse to higher coordinated sites to reduce the surface energy. In addition, above the critical potential the oxygen stemmed from the aqueous electrolyte solution is replaced by a Pt atom within the sublayers, resulting in an enhancement of surface roughness. The surface roughness leads to an enhanced surface disordering of the NCs with (100)-exposed surface.

We can sum up that the transformation of Pt NCs into a thermodynamically stable near-spherical shape is almost inevitable when the capping agent is entirely removed. The driving force for structural losses of NCs is the oxidation rate of capping agent which can be controlled by applied potential, number of cycles and scan rate.

3. Conclusion

The effect of capping agents (PVP and oleylamine) on the formation process, ORR activities as well as electrochemical and structural stability of Pt NCs was investigated in this work. Based on HR-TEM analysis, we determined the mono-dispersity of both PVP- and OAm-capped NCs to be 65% and 88%, respectively. However, the mean edge length of OAm-capped NCs was larger (9.3 ± 1.8 nm) than that for PVP-capped NCs (6.5 ± 0.5 nm). After washing, PVP and oleylamine as capping agent remain at the particle surface and might block the catalytically active Pt sites for the ORR. The chemical purity of

© 2019 The Authors. Published by Wiley-VCH Verlag GmbH & Co. KGaA

the Pt NCs was analyzed by EDX, whereby the PVP- and OAm-capped NCs contain less than 1 at.% Ag and about 5 at.% W, respectively. From XPS data, we figured out that the chemical state of Ag and W species is in form of oxides and/or chlorides. Despite its lower surface area-to-volume ratio, the OAm-capped NCs show higher ECSA and ORR activities (MA and SA) than the PVP-capped NCs. The improved catalytic ORR performance is related to the moderate adsorption behavior of oleylamine compared to the PVP polymer. Thus, the Pt(100)-preferred surface orientation is more exposed for the OAm-capped NCs in 0.1 M H_2SO_4, while the PVP strongly blocks the particle surface. Harsh post-treatment is needed to entirely remove the strongly adsorbed PVP from the Pt NC surface without any loss of the particle shape. Although the catalytic performance of the OAm-capped Pt NCs is very promising at the begin-of-life, they strongly suffer from the electrochemical cycling towards the upper potential of 1.2 V/RHE. A transformation from the cubic particle shape towards thermodynamically stable spherical shape occurs. The poor structural stability is accompanied by the quick loss of catalytic performance. Unlike, the initial particle shape of the PVP-capped NCs mainly prevails after the accelerated stress test protocol (2,000 cycles between 0.06–1.2 V/RHE). Due to the strong capping behavior of the PVP, only moderate changes of the ORR performance and ECSA for the PVP-capped Pt NCs were observed. From the structural stability results, an electrochemical-dependent particle shape degradation model for OAm- and PVP-capped NCs was developed. Our degradation model highlights the loss of edge and corner atoms as the origin of the shape loss, followed by transforming into a rounded cube and finally to a thermodynamically stable near-spherical shape. Tuning the adsorption strength of capping agent enables to improve the electrochemical ORR performance and structural stability of shape-controlled nanoparticles.

Acknowledgements

Financial support from the German Federal Ministry of Education and Research (BMBF, FKZ 03SF0539) is gratefully acknowledged. Furthermore, the funding of the JEOL JEM2100F HR-TEM, XPS and XRD measurements by the DFG (INST 184/106-1 FUGG, INST 184/154-1 FUGG) is acknowledged. Our appreciation goes to Dr. Volker Steenhoff of DLR – Institute of Network Energy Systems, Oldenburg, Germany, for his assistance with the FTIR measurements.

Conflict of Interest

The authors declare no conflict of interest.

Keywords: oleylamine, oxygen reduction reaction · polyvinylpyrrolidone · Pt nanocubes · shape stability

[1] S. Sui, X. Wang, X. Zhou, Y. Su, S. Riffat, C.-J. Liu, *J. Mater. Chem. A.* **2017**, *5*, 1808–1825.
[2] M. Oezaslan, F. Hasché, P. Strasser, *J. Phys. Chem. Lett.* **2013**, *4*, 3273–3291.
[3] M. Oezaslan, M. Heggen, P. Strasser, *J. Am. Chem. Soc.* **2012**, *134*, 514–524.
[4] H. A. Gasteiger, S. S. Kocha, B. Sompalli, F. T. Wagner, *Appl. Catal. B* **2005**, *56*, 9–35.
[5] J. Wang, H. Wang, Y. Fan *Engineering.* **2018**, *4*, 352–360.
[6] Y.-J. Wang, W. Long, L. Wang, R. Yuan, A. Ignaszak, B. Fang, D. P. Wilkinson, *Energy Environ. Sci.* **2018**, *11*, 258–275.
[7] X. Zhang, Z. Xia, Y. Huang, Y. Jia, X. Sun, Y. Li, X. Li, R. Wu, A. Liu, X. Qi, S. Wang, W. Wen, *Sci. Rep.* **2016**, *6*, 31404.
[8] S. I. Lim, I. Ojea-Jimenez, M. Varon, E. Casals, J. Arbiol, V. Puntes, *Nano Lett.* **2010**, *10*, 964.
[9] L. Gan, M. Heggen, S. Rudi, P. Strasser, *Nano Lett.* **2012**, *12*, 5423–5430.
[10] H. Lee, S. E. Habas, S. Kweskin, D. Butcher, G. A. Somorjai, P. D. Yang, *Angew. Chem. Int. Ed.* **2006**, *45*, 7824.
[11] K. M. Bratlie, H. Lee, K. Komvopoulos, P. D. Yang, G. A. Somorjai, *Nano Lett.* **2007**, *7*, 3097.
[12] I. Lee, F. Delbecq, R. Morales, M. A. Albiter, F. Zaera, *Nat. Mater.* **2009**, *8*, 132.
[13] Y. Kang, J. B. Pyo, X. Ye, R. E. Diaz, T. R. Gordon, E. A. Stach, C. B. Murray, *ACS Nano.* **2013**, *7*, 645–653.
[14] N. M. Markovic, P. N. Ross Jr, *Surf. Sci. Rep.* **2002**, *45*, 117–229.
[15] Y. N. Xia, Y. J. Xiong, B. Lim, S. E. Skrabalak, *Angew. Chem. Int. Ed.* **2009**, *48*, 60.
[16] J. Zhang, H. Yang, J. Fang, S. Zou, *Nano Lett.* **2010**, *10*, 638.
[17] Z. L. Wang, T. S. Ahmad, M. A. ElSayed, *Surf. Sci.* **1997**, *380*, 302.
[18] J. Zhang, J. Y. Fang, *J. Am. Chem. Soc.* **2009**, *131*, 18543.
[19] H. Song, F. Kim, S. Connor, G. A. Somorjai, P. D. Yang, *J. Phys. Chem. B.* **2005**, *109*, 188.
[20] M. A. Montiel, F. J. Vidal-Iglesias, V. Montiel, J. Solla-Gullón, *Curr. Opin. Electrochem.* **2017**, *1*, 34–39.
[21] D. Li, C. Wang, D. S. Strmcnik, D. V. Tripkovic, X. Sun, Y. Kang, M. Chi, J. D. Snyder, D. van der Vliet, Y. Tsai, V. R. Stamenkovic, S. Sun, N. M. Markovic, *Energy Environ. Sci.* **2014**, *7*, 4061–4069.
[22] I. A. Safo, C. Dosche, M. Oezaslan, *Z. Phys. Chem.* **2018**, *232*, 1319.
[23] D. Li, C. Wang, D. Tripkovic, S. Sun, N. M. Markovic, V. R. Stamenkovic, *ACS Catal.* **2012**, *2*, 1358–1362.
[24] F. Hasché, M. Oezaslan, P. Strasser, *ChemPhysChem.* **2012**, *13*, 828–834.
[25] I. A. Safo, M. Oezaslan, *Electrochim. Acta.* **2017**, *241*, 544–552.
[26] M. Crespo-Quesada, J.-M. Andanson, A. Yarulin, B. Lim, Y. Xia, L. Kiwi-Minsker, *Langmuir.* **2011**, *27*, 7909–7916.
[27] B. Gehl, A. Frömsdorf, V. Aleksandrovic, T. Schmidt, A. Pretorius, J.-I. Flege, S. Bernstorff, A. Rosenauer, J. Falta, H. Weller, M. Bäumer, *Adv. Funct. Mater.* **2008**, *18*, 2398–2410.
[28] N. Naresh, F. G. S. Wasim, B. P. Ladewig, M. Neergat, *J. Mater. Chem. A.* **2013**, *1*, 8553–8559.
[29] L. R. Baker, G. Kennedy, J. M. Krier, M. Van Spronsen, R. M. Onorato, G. A. Somorjai, *Catal. Lett.* **2012**, *142*, 1286–1294.
[30] K. M. Koczkur, S. Mourdikoudis, L. Polavarapu, S. E. Skrabalak, *Dalton Trans.* **2015**, *44*, 17883–17905.
[31] Z. Q. Niu, Q. Peng, Z. B. Zhuang, W. He, Y. D. Li, *Chem. Eur. J.* **2012**, *18*, 9813.
[32] N. V. Long, M. Ohtaki, M. Nogami, T. D. Hien, *Colloid Polym. Sci.* **2011**, *289*, 1373–1386.
[33] S. Mourdikoudis, L. M. Liz-Marzán, *Chem. Mater.* **2013**, *25*, 1465–1476.
[34] R. M. Arán-Ais, F. J. Vidal-Iglesias, J. Solla-Gullón, E. Herrero, J. M. Feliu, *Electroanalysis* **2015**, *27*, 945–956.
[35] I. A. Safo, M. Werheid, C. Dosche, M. Oezaslan, *Nanoscale Adv.* **2019**, *1*, 3095–3106.
[36] C. Wang, H. Daimon, Y. Lee, J. Kim, S. Sun, *J. Am. Chem. Soc.* **2007**, *129*, 6974–6975.
[37] R. Gómez, J. M. Orts, B. Álvarez-Ruiz, J. M. Feliu, *J. Phys. Chem. B.* **2004**, *108*, 228–238.
[38] Y. Borodko, S. E. Habas, M. Koebel, P. Yang, H. Frei, G. A. Somorjai, *J. Phys. Chem. B.* **2006**, *110*, 23052–23059.
[39] L. Qiu, F. Liu, L. Zhao, W. Yang, J. Yao, *Langmuir.* **2006**, *22*, 4480–4482.
[40] A. M. Ferraria, A. P. Carapeto, A. M. Botelho do Rego, *Vac.* **2012**, *86*, 1988–1991.
[41] D. Tamboli, S. Seal, V. Desai, A. Maury, *J. Vac. Sci. Technol.* **1999**, *17*, 1168–1173.
[42] S. S. Perry, H. C. Galloway, P. Cao, E. J. R. Mitchell, D. C. Koeck, C. L. Smith, M. S. Lim, *Appl. Surf. Sci.* **2001**, *180*, 6–13.

© 2019 The Authors. Published by Wiley-VCH Verlag GmbH & Co. KGaA

[43] W. Banerjee, S. Maikap, C.-S. Lai, Y.-Y. Chen, T.-C. Tien, H.-Y. Lee, W.-S. Chen, F. T. Chen, M.-J. Kao, M.-J. Tsai, J.-R. Yang, *Nanoscale Res. Lett.* **2012**, *7*, 194.
[44] C. Peniche, D. Zaldívar, M. Pazos, S. Páz, A. Bulay, J. S. Román, *J. Appl. Polym. Sci.* **1993**, *50*, 485–493.
[45] F. C. C. Oliveira, F. B. Effenberger, M. H. Sousa, R. F. Jardim, P. K. Kiyohara, J. Dupont, J. C. Rubim, L. M. Rossi, *Phys. Chem. Chem. Phys.* **2011**, *13*, 13558–13564.
[46] J. J. L. Humphrey, S. Sadasivan, D. Plana, V. Celorrio, R. A. Tooze, D. J. Fermín, *Chem. Eur. J.* **2015**, *21*, 12694–12701.
[47] R. M. Arán-Ais, J. Solla-Gullón, E. Herrero, J. M. Feliu, *J. Electroanal. Chem.* **2018**, *808*, 433–438.
[48] J. Clavilier, D. Armand, *J. Electroanal. Chem. Interfacial Electrochem.* **1986**, *199*, 187–200.

Manuscript received: July 1, 2019
Revised manuscript received: August 26, 2019
Accepted manuscript online: September 19, 2019
Version of record online: October 14, 2019

© 2019 The Authors. Published by Wiley-VCH Verlag GmbH & Co. KGaA